ACS APPLIED MATERIALS & INTERFACES

Research Article

www.acsami.org

Adherent and Conformal Zn(S,O,OH) Thin Films by Rapid Chemical Bath Deposition with Hexamethylenetetramine Additive

Borirak Opasanont,[†] Khoa T. Van,[†] Austin G. Kuba,[†] Kaushik Roy Choudhury,[‡] and Jason B. Baxter*[,†]

[†]Chemical and Biological Engineering Department, Drexel University, Philadelphia, Pennsylvania 19104, United States

[‡]Central Research and Development, DuPont Experimental Station, Wilmington, Delaware 19803, United States

Supporting Information

ABSTRACT: ZnS is a wide band gap semiconductor whose many applications, such as photovoltaic buffer layers, require uniform and continuous films down to several nanometers thick. Chemical bath deposition (CBD) is a simple, low-cost, and scalable technique to deposit such inorganic films. However, previous attempts at CBD of ZnS have often resulted in nodular noncontinuous films, slow growth rates at low pH, and high ratio of oxygen impurities at high pH. In this work, ZnS thin films were grown by adding hexamethylenetetramine (HMTA) to a conventional recipe that uses zinc sulfate, nitrilotriacetic acid trisodium salt, and thioacetamide. Dynamic bath characterization showed that HMTA helps the bath to maintain near-neutral pH and also acts as a catalyst, which leads to fast nucleation and deposition rates, continuous films, and less oxygen impurities in the films. Films deposited on glass from HMTA-containing bath were uniform, continuous, and 90 nm thick after 1 h, as opposed to films grown without HMTA that were ∼3 times thinner and more nodular. On $Cu_2(Zn,Sn)Se_4$, films grown with HMTA were continuous within 10 min. The films have comparatively few oxygen impurities, with S/(S + O) atomic ratio of 88%, and high optical transmission of 98% at 360 nm. The Zn(S,O,OH) films exhibit excellent adhesion to glass and high resistivity, which make them ideal nucleation layers for other metal sulfides. Their promise as a nucleation layer was demonstrated with the deposition of thin, continuous Sb_2S_3 overlayers. This novel HMTA chemistry enables rapid deposition of Zn(S,O,OH) thin films to serve as a nucleation layer, a photovoltaic buffer layer, or an extremely thin continuous coating for thin film applications. HMTA may also be applied in a similar manner for solution deposition of other metal chalcogenide and oxide thin films with superior properties.

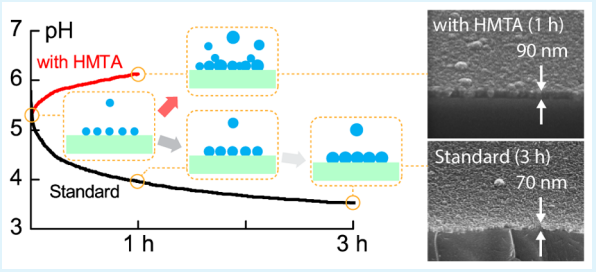

KEYWORDS: *chemical bath deposition, zinc sulfide, thin film, buffer layer, nucleation, hmta*

INTRODUCTION

Many applications require uniform and continuous films with thickness control down to nanometers. Chemical bath deposition (CBD) is a simple, low-cost, and scalable technique for depositing inorganic thin films, but forming a thin, continuous and uniform film by CBD is highly dependent on the degree of nucleation and the surface properties.[1] While the film nucleation process is still not fully understood or reliably quantifiable, some general observations have been made. Surfaces with higher energy, from defects, charge, or impurities, tend to allow more facile nucleation or attachment of nuclei.[2] The same can be said for surfaces with chemical similarity to the depositing material, likely because of similar crystal structure, lattice matching, or nature of the bonds.[3] Glass and SnO_2:F (fluorine-doped tin oxide, FTO) are low-cost substrates commonly used for optical characterization of thin films because of their high transparency. These substrates are oxides and have low surface defect density (amorphous for glass and relatively high crystallinity for FTO). Difficulty in nucleation of non-oxides leads to nodular, noncontinuous deposits, thus making optical or electrical characterization of these films challenging.

ZnS is a semiconductor with a wide band gap of 3.6 eV; it has vast potential application in thin film devices such as luminescents[4] and buffer layers in heterojunction solar cells.[5,6] Unfortunately, deposition of thin yet continuous ZnS films from solution has proven to be a great challenge because homogeneous nucleation typically dominates compared to heterogeneous nucleation.[1] The nuclei formed in solution then aggregate to form clusters and deposit on the substrate.[7] However, by carefully controlling the starting bath parameters and, more importantly yet often neglected, their time evolution, rapid and continual nucleation can occur and enable fast deposition of continuous films. Additionally, since ZnS has high electrical resistivity and is chemically similar to other sulfides, a thin and continuous layer of nanocrystalline ZnS is an ideal candidate as a nucleation layer on glass or FTO to overcome this challenge for other sulfide films such as Sb_2S_3.[8,9]

In this work, ZnS thin films were deposited in a near-neutral pH regime. CBD-grown ZnS films often include oxygen in form of oxide and hydroxide and are more appropriately called

Received: March 20, 2015
Accepted: May 8, 2015
Published: May 8, 2015

DOI: 10.1021/acsami.5b02482
ACS Appl. Mater. Interfaces 2015, 7, 11516−11525

Zn(S,O,OH). Oxide decreases the band gap to as low as 2.6 eV,[10] while hydroxide is regarded as an instability. Lower overall oxygen content in the film is therefore desirable. In alkaline Zn(S,O,OH) deposition, oxygen inclusion can yield S/(S + O) atomic ratios as low as 0.42.[11] Deposition at lower pH should yield less oxygen since the ZnO and $Zn(OH)_2$ phases are undersaturated versus their solubility products, but deposition rates are slow. Here, deposition was performed under near-neutral pH conditions because they provide sufficiently fast reaction rates with the thioacetamide (TAA) sulfur source and potentially reduce oxygen inclusion.

In the near-neutral pH regime, direct reaction of Zn and TAA dominates the precipitation rate, as opposed to the free ion reaction in the alkaline or acidic regimes, and the rate increases with pH according to[12]

$$-\frac{d[Zn^{2+}]}{dt} = k\frac{[Zn^{2+}][TAA]}{[H^+]^{1/2}}$$

where k is the rate constant and square brackets indicate concentrations. Subsequently, film deposition rate was found to be linearly correlated to this precipitation rate.[7] TAA consumes OH^- (or, equivalently, generates H^+) as it undergoes hydrolysis, reducing the pH and deposition rate with time. To maintain high pH and reaction rate, hexamethylenetetramine (HMTA) was added to the bath. HMTA is widely used in CBD of ZnO as a pH controller in the near-neutral region through slow release of ammonia. We have previously shown that HMTA does not complex with Zn, and addition of HMTA should not reduce the free Zn^{2+} ion concentration.[13] Instead, addition of HMTA should significantly increase the deposition rate by maintaining moderate pH to provide rapid and continual nucleation followed by accelerated growth.

We deposited Zn(S,O,OH) thin films by CBD with HMTA as an additive (HMTA films) and compared them to standard films without the bath additive. Well-adherent, uniform, and continuous HMTA films were successfully deposited on glass and FTO at ~90 nm thick in 1 h, which is ~3 times faster than standard films. As a potential buffer layer, HMTA film achieved total coverage in 10 min of deposition, with thickness of ~10 nm, on $Cu_2(Zn,Sn)Se_4$ (CZTSe) substrates. The films showed high optical clarity, low oxygen content, and low strain. High electrical resistivity and excellent adhesion make the film suitable as a nucleation layer for other metal sulfides, which we demonstrated by deposition of a thin, continuous Sb_2S_3 film. The addition of HMTA provides a pathway for potential improvements to CBD of thin films through tailoring the evolution of the chemical bath.

EXPERIMENTAL DETAILS

Film Deposition. Soda-lime glass (Hartford Glass) and SnO_2:F on glass (FTO; TEC15, Pilkington) substrates cut to 25 mm × 60 mm were cleaned by sequential sonication at 60 °C for 15 min in 20% Contrad 70 (Decon Laboratories), acetone−ethanol solution, and 1 M HCl, followed by multiple rinses in deionized (DI) water (18.2 MΩ·cm, Barnstead) and drying under nitrogen stream. CZTSe substrates were used as received from DuPont.[14]

For deposition of standard film, stock solutions of 0.40 M $ZnSO_4$ and 0.40 M nitrilotriacetic acid trisodium salt (NTA) were used. NTA was chosen as the ligand over ethylenediaminetetraacetic acid (EDTA) because we have observed the former to maintain high deposition rates for longer times. All chemicals were of ACS reagent grade and were used as obtained from Sigma−Aldrich without further purification. Three containers were used in preparing the precursor solutions: a glass beaker filled with 15 mL of $ZnSO_4$ solution and 45 mL of deionized water, a bottle filled with 15 mL of NTA solution and 30 mL of DI water, and another bottle of 45 mL of 0.40 M aqueous thioacetamide (TAA) solution. The precursor solutions were separately heated in a stirred water bath at 90 °C for 8 min. To improve adhesion, substrates were preheated in $ZnSO_4$ solution. NTA and TAA solutions were then added to the beaker in that order under vigorous stirring, resulting in 150 mL of reacting solution with 0.040 M $ZnSO_4$, 0.040 M NTA, and 0.120 M TAA. The recipe is an adaptation from the works of Goudarzi et al.[15] and Shin et al.[16] but with NTA replacing EDTA. Reaction took place at 90 °C for up to 3 h in the beaker covered with aluminum foil. Finally, substrates were rinsed with DI water at room temperature and dried under a stream of nitrogen gas.

For deposition of HMTA film, three containers were also used in preparation of the precursor solutions: a beaker containing 15 mL of $ZnSO_4$ solution, 15 mL of NTA solution, 0.450 mL of concentrated H_2SO_4 (Fisher Scientific), and 30 mL of DI water; a bottle of 45 mL of 0.40 M TAA; and a bottle of 45 mL of 1.0 M HMTA. The acid was used to adjust the starting pH to ~5.2 (at 90 °C). Too-high pH results in abrupt nucleation and poor film growth, while too-low pH leads to slow deposition. The HMTA concentration is selected for fastest film growth, although smaller amounts may be used. Both TAA and HMTA solutions were freshly made from powder before each use. The precursor solutions were preheated similar to the standard bath. TAA and HMTA were added to the beaker at the same time under vigorous stirring, resulting in a reacting solution of similar composition as the standard bath but with 0.30 M HMTA. The reaction took place at 90 °C for up to 1 h. Substrates need not be preheated for excellent adhesion. In addition to the DI water rinse, an acetone rinse was necessary to remove organic residues from the film surface.

Film Characterization. Zn(S,O,OH) thin films were imaged by scanning electron microscopy (SEM, Zeiss Supra 50VP) at 15 kV and working distance of ~4 mm with in-lens detector. Film thickness measurements were obtained from cross-sectional micrographs of the films.

Optical transmission measurements were done on a Thermo Genesys 10S UV−vis spectrophotometer in scanning mode with monochromator step size of 0.5 nm and beam spot size of 2 mm × 7 mm.

X-ray photoelectron spectroscopy (XPS) measurements were performed on a Physical Electronics VersaProbe 5000 instrument with a monochromatic Al Kα X-ray source operated at 15 kV and 25 W. The X-ray spot size was 100 μm. Survey and detailed spectra were collected with pass energy of 117.4 and 23.5 eV, respectively. Surface contaminants were removed from the films by argon sputtering at 1 kV within an area 2 mm × 2 mm for 30 s under ultra-high-vacuum (UHV) conditions, and depth profiling was achieved with the same gun settings at 1 min intervals. Data analysis and peak fitting were performed with CasaXPS software with relative sensitivity factors as recommended by the equipment manufacturer. Linear backgrounds were used since the films have insulating characteristics. Spectral shifts were corrected by use of the C−C/C−H 1s peak at 284.5 eV and confirmed with the Zn 2p peak at 1021.8 ± 0.1 eV.

Grazing-incidence X-ray diffraction (GIXRD) was done on Zn(S,O,OH) films on glass at incidence angle of 0.3° and spot size of 15 mm by use of a Rigaku SmartLab diffractometer equipped with Cu Kα X-ray source operated at 40 kV and 44 mA and parallel beam, in-plane optics. A scan rate of 0.0280°/min and step size of 0.05° were used.

Electrical resistivity measurements were made with a metal-insulator-metal structure in a dark Faraday's cage at room temperature on a Keithley 2634B instrument. Films were deposited on conductive FTO (15 Ω/sq), and an apertured area of 0.318 cm^2 was covered with conductive silver paint (SPI Supplies, <100 mΩ/sq) or thermally evaporated silver of ~100 nm thickness. Contacts were checked for Ohmic behavior by sweeping voltages between −100 and 100 mV. At least five devices were tested per film type.

For adhesion measurement, films were deposited on the 2.2 mm thick glass substrates. An identical glass piece was bonded to the film side via a layer of 5-min epoxy (Loctite). A Kapton tape−Teflon shim

DOI: 10.1021/acsami.5b02482
ACS Appl. Mater. Interfaces 2015, 7, 11516−11525

stack was inserted on one end before the epoxy application to create a precrack allowance. Epoxy was chosen as it adheres to the cover glass and the film extremely well and will not fracture before the film–substrate interface. The epoxy layer was orders of magnitude thinner than the glass beams, and thus the Young's moduli of the beams can be assumed to be that of the glass beams alone (and hence symmetrical). Film adhesion was tested by applying a perpendicular displacement to the interface at one end by use of a razor blade and measuring the crack length propagated parallel to the beams.

Bath Characterization. Attenuated total reflectance Fourier transform infrared spectroscopy (ATR-FTIR) measurements were performed on a Thermo Electron Nicolet 6700 series FTIR spectrometer. For bath composition study, aliquots were extracted from the baths at 5 min intervals, filtered with 0.45 μm syringe filter, quenched to room temperature in an ice bath, and drop-cast onto the diamond ATR (Specac Inc.) with spot size of 2 mm × 2 mm. All spectra were collected by use of a liquid nitrogen-cooled mercury–cadmium–telluride (MCT) detector with 32 scans/spectrum at a resolution of 4 cm^{-1}. A background spectrum of the bare ATR crystal was collected and subtracted from all measurement spectra. The spectra were further corrected by subtracting an appropriate weighting of the water spectrum.

The bath pH was measured with a pH probe (Thermo Orion 8102BNUWP), preheated and calibrated at 90 °C with NIST pH 4, 7, and 10 standards connected to a meter (Thermo Orion 4-Star pH/ISE). For bath sulfide concentration, preparation and measurement were performed similarly to the methods previously reported.[11,17] Aliquots were extracted at 5 min intervals, filtered with 0.45 μm syringe filter, collected in individual containers preloaded with chilled sulfide antioxidant buffer (SAOB) solution, and stabilized in a room-temperature water bath. A silver/sulfide ion-selective electrode (ISE, Oakton WD-35802-40) connected to a standard microvolt meter was used for the measurement. Details of the preparation of SAOB and calibration of sulfide concentration to voltage reading are provided in Supporting Information.

RESULTS AND DISCUSSION

The decomposition of HMTA releases formaldehyde and ammonia and leads to an increase in bath pH according to the reactions

$$C_6H_{12}N_4 + 6H_2O \rightleftharpoons 6CH_2O + 4NH_3$$

and

$$NH_3 + H_2O \rightleftharpoons NH_4^+ + OH^-$$

The formaldehyde is believed to be inactive in the deposition of Zn(S,O,OH). However, it may be involved in reactions that form a small amount of insoluble organic residue that segregates at the bath–air interface after long reaction times. Upon sample removal from the bath, the organic residues loosely attached onto the surface of the film, requiring an acetone rinse.

In the standard bath, the pH started at 5.5 as shown in Figure 1 and decreased to 3.5 after 3 h due to consumption of OH^- in the decomposition of TAA. Addition of HMTA to the bath requires addition of an acid to keep the starting pH moderate and nucleation at a suitable pace. The pH of the HMTA bath started at ∼5.2, about the same as the standard bath, but increased rapidly to 5.8 in 15 min, then steadily to 6.1 after 1 h and even higher at longer times. The higher pH and other effects of HMTA on the deposition of Zn(S,O,OH) thin films are discussed next.

Film Properties. For many applications, thin films should be compact, uniform, continuous, and excellently adherent to the substrate. Figure 2 shows tilt view SEM micrographs of (a) 1 h and (b) 3 h standard films on glass. The 1 h film has

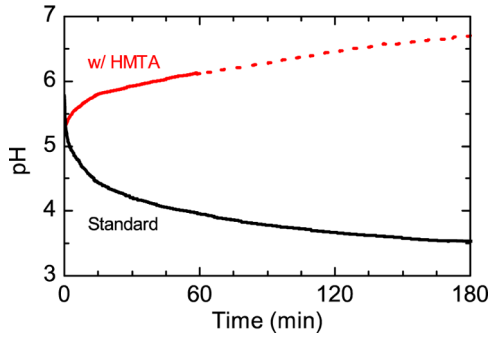

Figure 1. pH profile in standard and HMTA baths as a function of time. In the standard bath, thioacetamide decomposition consumes hydroxide ions, and pH decreases with time. In the HMTA bath, thermal decomposition of HMTA leads to an increase in hydroxide ions in the bath. pH increases even further after 60 min as denoted by the dotted line.

noncontinuous nodules of uniform ∼20 nm size on the glass substrate, whereas the 3 h film fully covers the substrate with thickness of ∼70 nm as measured by cross-sectional SEM. The nodules are reasonably monodisperse, which suggests an impulse-like nucleation phase during the high-pH period, followed by a separate growth phase. It is unclear whether nodule nucleation originated heterogeneously or in the solution. With the presence of HMTA, film formation started at earlier times of ∼15 min (Figure 2c). Unlike the standard film at the early stage, the HMTA film has nodules with wide size distribution of 20–60 nm, which suggests continual nucleation followed by aggregation or growth. The film is continuous and uniform after 1 h of deposition with thickness of ∼90 nm (Figure 2d), approximately 3× faster than the time required for continuous standard film. On CZTSe, HMTA film started coverage at just 2 min, and required only 10 min to achieve a continuous 10–20 nm thick film (Figure 2e,f; XPS surface coverage data are shown in Figure S1 in Supporting Information). Standard films tended to flake off if they were not preheated in $ZnSO_4$ solution. HMTA films did not require such treatment and adhered to the glass substrates well. The 3 h standard and 1 h HMTA films on glass were used for further characterization.

In addition to morphology, stoichiometry critically influences the functional properties of the ZnS films. Oxygen has been widely observed in chemical bath deposited ZnS thin films and is typically found as oxide or hydroxide. The inclusion of oxide can reduce the band gap of the film to as low as 2.6 eV,[10] while the presence of hydroxide is often regarded as an instability. Therefore, less oxygen is preferred in order to maintain high band gap and transparency. The presence of oxygen in the films is confirmed by XPS analysis, as shown in the depth profiles of standard and HMTA films in Figure 3. Conductive FTO was used as the substrate instead of glass to minimize charge buildup on the sample during measurements. The sulfur–oxygen composition is reported as S/(S + O) atomic ratio. Less oxygen is found in the HMTA film with bulk S/(S + O) of 0.88 ± 0.01 as compared to the standard film at 0.80 ± 0.01.

Detailed XPS spectra contain rich information about the states and environment of each constituent element to provide insight into likely contaminants in the films. Besides oxide and hydroxide, detailed O 1s spectra reveal an additional peak at 533.5 eV for both films (Figure 4a), which contributes <1% of the total film content and decreases with depth of sputter. This

DOI: 10.1021/acsami.5b02482
ACS Appl. Mater. Interfaces 2015, 7, 11516–11525

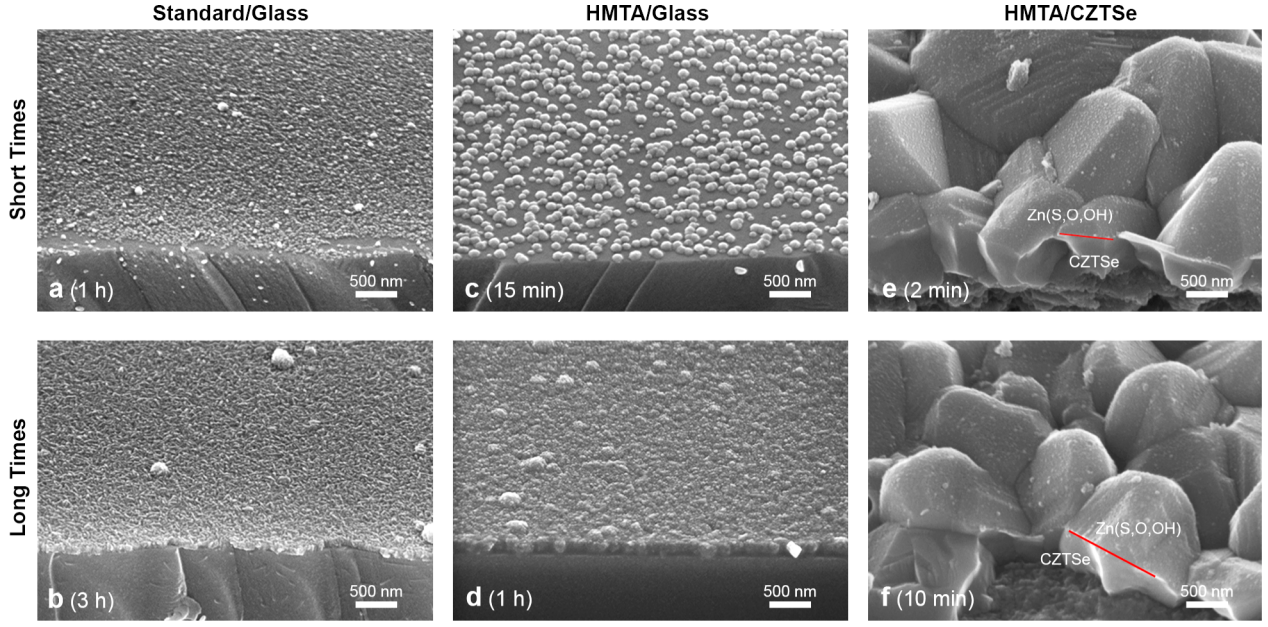

Figure 2. (a, b) Tilt view of scanning electron micrographs of standard film at (a) 1 h and (b) 3 h of deposition on glass. At the shorter time, film consists of uniform nodules, suggesting impulse nucleation, and is not continuous. At 3 h, the film is continuous and is ∼70 nm thick. (c, d) For the HMTA film on glass at 15 min (c), coverage is incomplete, and the wide nodule size distribution suggests continual nucleation. After 1 h (d), the HMTA film is uniform and continuous with thickness ∼90 nm. (e, f) On CZTSe, the HMTA film started coverage at just 2 min (e) and is fully continuous over the large CZTS grains in 10 min (f).

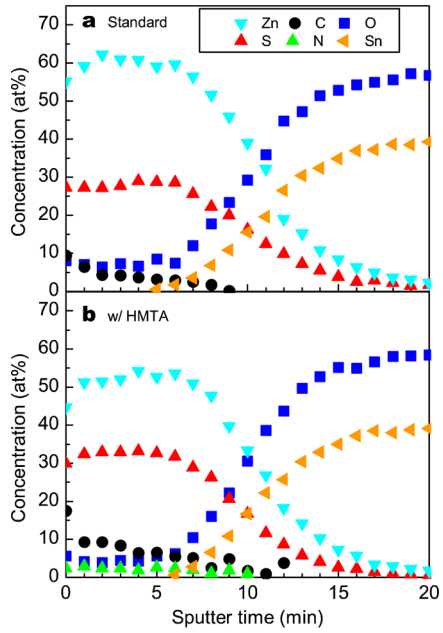

Figure 3. Depth profile of atomic composition of (a) standard and (b) HMTA films on FTO substrate as determined by X-ray photoelectron spectroscopy. HMTA film contains ∼2% nitrogen and significantly higher amount of carbon but also higher sulfur fraction.

peak is assigned to the carbonyl O peak,[18] which is likely from NTA. NTA binds strongly to Zn^{2+} and may have also been incorporated into the films. Other evidence of the inclusion of NTA includes the presence of carbon in the bulk film, at ratios of 5% in standard film and 10% in HMTA film. Detailed C 1s spectra (Figure 4b) show C−C/C−H, C−N/C−S, and COOH peaks in both films, further supporting the presence of NTA. In addition, the ratio of C−N/C−S peak to the C−C/C−H peak is significantly higher in the HMTA film than the standard film, suggesting that NTA is not the only impurity in the HMTA film. Nitrogen of ∼2% is also detected in the case of HMTA but is not present at a detectable level in the standard case. These observations suggest the inclusion of NCS^- or TAA into the HMTA film. HMTA itself is unlikely to be incorporated into the film as it does not bind to Zn.[19] Each S 2p spectrum is best fitted with a doublet with 1:2 intensity ratio and equal full width at half-maximum (fwhm), at 161.5 eV (Figure 4c), indicating that the only oxidation state of sulfur is −2, belonging largely to ZnS. The fwhm tightens with sputter depth, an expected result of decreasing amount of impurities. No sulfate peaks were detected at ∼170 eV.

Composition and morphology affect the transparency of the films, which is important for photovoltaic and optoelectronic applications. High-transparency films allow more photons to pass through and interact with underlying layers. Figure 5 shows UV−visible transmission spectra of standard and HMTA films, with the reference glass substrate subtracted. The HMTA film has higher transmission than the standard film at all wavelengths, as high as 98% versus 85% at 360 nm. The linear relationship between $(\alpha h\nu)^2$ and photon energy in the Tauc plot inset in Figure 5 shows that both films have direct band gaps. The HMTA film has a higher band gap of 3.75 eV as compared to 3.61 eV for the standard film, partly contributing to its higher transparency in the blue wavelength region. One of the possible reasons for the higher band gap is the higher sulfur fraction in the HMTA film than the standard film. However, the band gap of 3.75 eV is higher than literature values of crystalline ZnS at 3.6 eV,[20] suggesting that crystallite size quantization may have a more pronounced effect on band gap than the film composition.

Knowing the crystallite sizes and phases may help elucidate the difference in band gap of the films. Grazing-incidence XRD is a suitable technique for probing crystallinity of thin films as it probes only the top layer of the sample, minimizing

DOI: 10.1021/acsami.5b02482
ACS Appl. Mater. Interfaces 2015, 7, 11516−11525

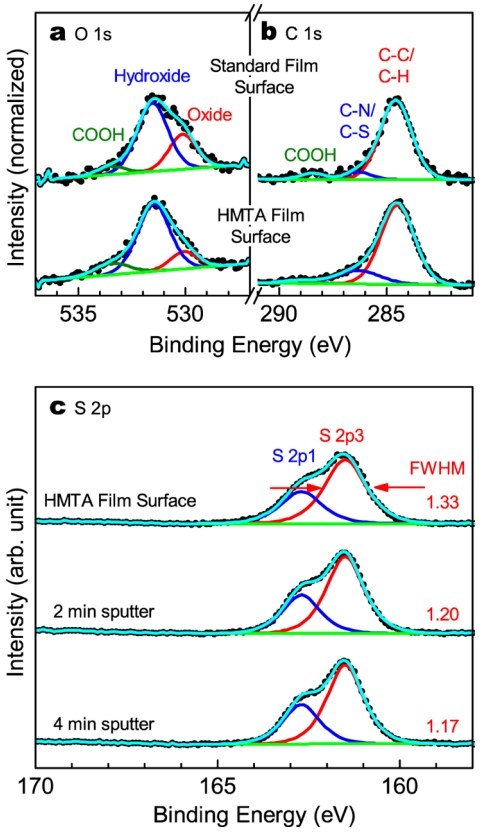

Figure 4. (a) Detailed XPS spectra of the O 1s region from film surfaces with additional carbonyl O peak at 533.5 eV in addition to the expected oxide and hydroxide peaks. (b) Spectra of the C 1s region showing higher C−N/C−S contribution to the overall carbon content of the HMTA film than the standard film. (c) S 2p spectra of the HMTA film are best fitted with a doublet of peaks. The full width at half-maximum (fwhm) narrows with depth, suggesting fewer impurities.

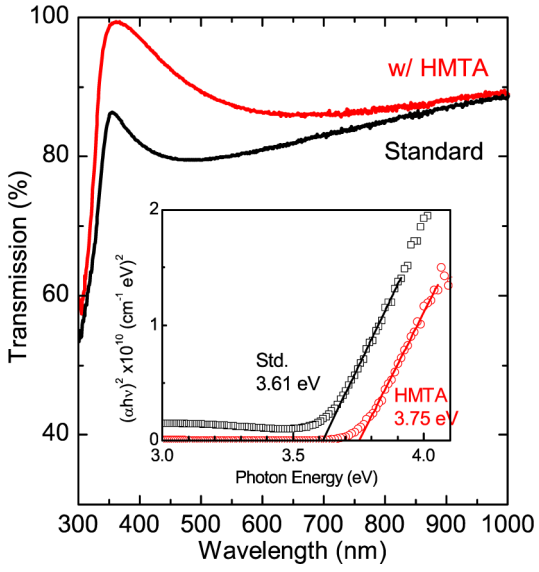

Figure 5. UV−vis transmission spectra showing greater transmission by HMTA film than standard film. (Inset) Tauc plot shows direct band gaps of 3.61 eV for the standard film and 3.75 eV for the HMTA film.

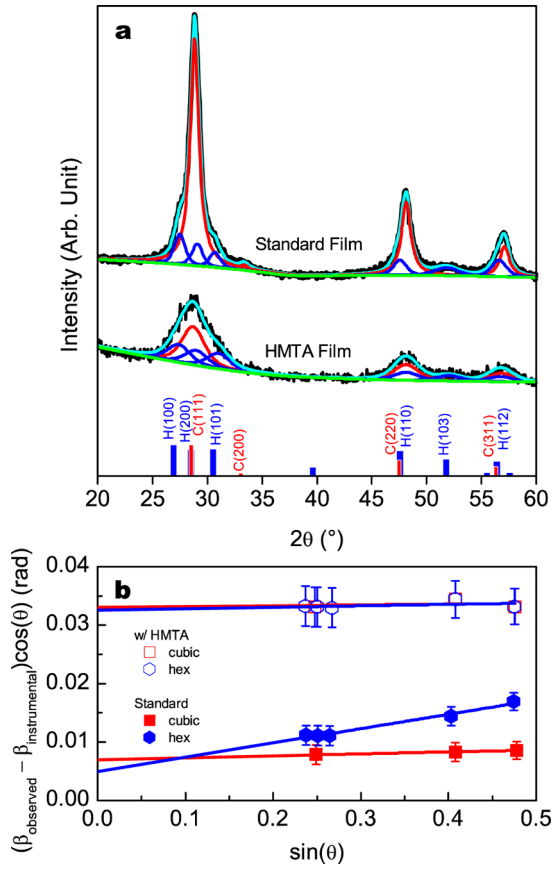

Figure 6. (a) Grazing-incidence X-ray diffractograms of standard and HMTA films on glass. Vertical bars show relative intensities for hexagonal ZnS (PDF 00-036-1450) and cubic ZnS (PDF 01-077-2100). Peaks were fitted with pseudo-Voigt line shapes and their full widths at half-maximum (β_{obs}) were extracted. (b) Williamson−Hall plot showing that the hexagonal component of the standard film has greater strain (slope) than its cubic counterpart and the HMTA film.

interference from the substrate. GIXRD diffractograms of standard and HMTA films on glass are shown in Figure 6a. The standard film, in general, has peaks with tighter fwhm than the HMTA film. The peak centered at $2\theta \sim 28.8°$ has obvious asymmetry, which indicates the presence of multiple components, and thus all peaks were fitted with pseudo-Voigt line shape components. The relative heights of the component peaks largely resemble those in the powder diffraction file database, PDF 00-036-1450 for hexagonal ZnS and PDF 01-077-2100 for cubic ZnS, which are depicted as vertical bars in Figure 6a, suggesting that there is no texturing or preferred orientation of the crystallites. The cubic-phase peaks are sharper and more intense than the hexagonal peaks, indicating larger quantity and size of the former phase. The peak positions can tell us about the lattice spacings. Both cubic and hexagonal phases have $0.5°(2\theta)$ shift toward larger 2θ, indicating that the average lattice spacing is smaller than pure ZnS phases, possibly due to the substitution of oxygen for sulfur.

Bragg peaks from ZnO and $Zn(OH)_2$ phases are not present at any position for either film, indicating that those species are not significantly present in crystalline form. The smaller diffraction intensities of HMTA versus standard film are possible indications of the former's higher amorphous content, given that they have similar film thicknesses. Annealing the HMTA film at 200 °C for up to 1 h in air did not change the

DOI: 10.1021/acsami.5b02482
ACS Appl. Mater. Interfaces 2015, 7, 11516−11525

diffractogram, indicating no improvements to its crystallinity or relative phase composition (see Figure S2 in Supporting Information).

Peak widths can reveal information about crystallite size and strain. Fwhm values of peaks were extracted from peaks with reliable signal-to-noise ratio and were plotted as a Williamson−Hall (W−H) plot for Lorentzian peak shape as shown in Figure 6b.[21] Modeling the W−H plot with a single peak shape provides insight into the properties of the materials with sufficient precision for our purposes. The W−H equation assumes linear combination of the effects of size and strain on peak broadening, β. Substituting Scherrer's size broadening equation and Stoke and Wilson's strain broadening equation as functions of θ, and rearranging, yields the expression

$$(\beta_{obs} - \beta_{instrum})\cos\theta = \left(\frac{k\lambda}{L}\right) + 4\varepsilon \sin\theta$$

where k = 0.94, λ = incident X-ray wavelength, L = average crystallite size, and ε = average strain. By plotting $(\beta_{obs} - \beta_{instrum})\cos\theta$ versus $\sin\theta$, the ordinate intercept and slope are used for determining crystallite size and strain, respectively. The crystallite sizes are 20 ± 6 nm and 30 ± 12 nm, respectively, for cubic and hexagonal phases of standard film. The cubic phase has strain ε = 0.083% ± 0.007%, while the hexagonal phase is roughly an order of magnitude higher with ε = 0.62 ± 0.05%. The two phases likely form together at the early stage, possibly as a mixed stacking similar to the observation in a precipitation study by Zhang et al.[22] A diffractogram of our standard film deposited with three sequential 1 h depositions showed higher hexagonal-cubic phase ratio as compared to the 3 h standard film (see Figure S2 in Supporting Information). Thus, growth of the cubic phase is likely favored over the hexagonal phase as the standard bath gets more acidic with time (see Figure 1); hence the greater diffraction intensities of the cubic peaks despite having somewhat similar crystallite sizes. This effect may have caused the extra strain on the hexagonal phase.

The component peaks of the HMTA film are less sharp than those of the standard film. Peak positions are shifted 0.4°(2θ) for cubic and 0.3°(2θ) for hexagonal phases toward larger 2θ, which are less than the shifts in the standard film. The smaller shifts indicate less degree of oxygen substitution with sulfur in the lattice, in agreement with the higher sulfur fraction observed by XPS. As with the standard film, there is no preferred crystallite orientation, with relative peak intensities similar to the powder references. W−H plot yields strain-free film within the limits of the method, with 0.0% ± 0.2% for cubic phase and 0.06 ± 0.07% for the hexagonal phase. Crystallite sizes for the cubic and hexagonal phases are each 4.4 ± 0.5 nm. Deposition of ZnS at near-neutral pH is rather well accepted to occur through the cluster-by-cluster mechanism, followed by aggregation of small clusters (~4 nm) to form larger grains (20−100 nm),[7] which agrees with our SEM observation at early time (Figure 2c). Unlike the standard film, these crystallite sizes are small and are likely to have contributed to the wider band gap of the HMTA film by the size quantization effect, more so than the effect of atomic composition.

One of the effects of ZnS having a wide band gap is the high electrical resistivity.[23] Resistivity measurements were performed by a two-contact sandwich method, suitable for insulating materials.[24] The HMTA film showed resistivity of 10^8~10^9 Ω·cm with conductive silver paint contacts and (2.2 ± 0.7) × 10^6 Ω·cm with thermally evaporated silver contacts. Annealing the film did not appreciably alter the resistivity values. The standard film showed a similar order of magnitude of resistivity as the HMTA film. These values are lower than the reported 10^8~10^{12} Ω·cm range in the literature for CBD-Zn-(S,O,OH)[23,25] but are still higher than many semiconductor materials, making the films suitable as nucleation layers for electrical testing of other thin films.

For a nucleation layer, adhesion to the substrate is important. A Scotch-tape test revealed that the HMTA film resisted peeling and adhered well to the glass substrate, while the standard film showed high variability, with some films remaining on the substrate but others peeling off with the tape. In order to quantify adhesion of the films, a double cantilever beam (DCB) test was employed. DCB tests are widely used for characterizing wafer bonding, an important manufacturing process for microelectronics.[26] The DCB test was conducted by inserting a thin blade at the interface of a bonded pair of beams and measuring the propagated crack length. Figure 7a illustrates the experimental setup where the glass substrate acted as the bottom beam, a similar glass cover was used as the top beam, and a layer of epoxy bonded the two. The equation relating crack length, L, to the work of adhesion, W_A, is given by the Maszara model equation:[27]

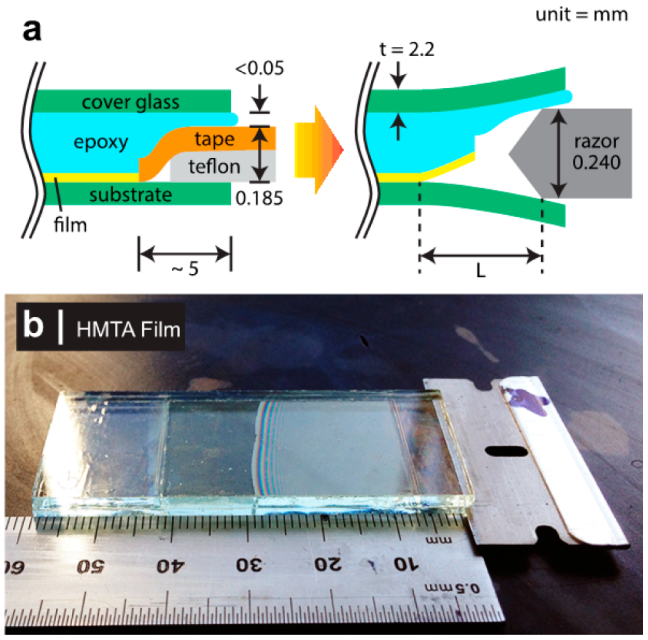

Figure 7. Double cantilever beam test for film surface fracture energy. (a) Specimen preparation and test schematic (not to scale). (b) HMTA film under test showing crack length of 29 mm.

$$W_A = \frac{3E\delta^2 t^3}{16L^4}$$

where E is the Young's modulus of the beam (72 GPa for soda-lime glass),[28] δ is the load-point displacement (difference between razor blade and shim stack thicknesses), and t is the beam thickness.

Figure 7b shows a photograph of the HMTA film under reflection of a visible light source. Crack fringes are visible due to light interaction with the submicrometer air gap. Observation by the naked eye after removing the cover glass

DOI: 10.1021/acsami.5b02482
ACS Appl. Mater. Interfaces 2015, 7, 11516−11525

confirmed that the interface fracture occurred at the film−substrate interface. The work of adhesion obtained from three samples of HMTA film was 0.72 ± 0.10 J/m^2, which is comparable to that of vacuum-deposited metals on glass[29] and graphene on copper.[30] Similar to the analyses in refs 29 and 30, we believe van der Waals forces contribute primarily to the work of adhesion, while other interactions such as electrostatic, ionic, and covalent bonding may also play a small role.

For standard films, results were highly varied with samples cracking to various lengths and some beyond the limit of the beam length, in agreement with the Scotch-tape test. The strain in the hexagonal phase of the film is a plausible reason for poor adhesion to the substrate.

Application as Nucleation Layer. Since the HMTA film can be deposited uniformly and adherently over glass and FTO and has high transparency and band gap, it is an ideal candidate for a nucleation layer for other metal sulfide films. Sb_2S_3 has gained much attention as a photovoltaic absorber material,[31,32] but studying the thin film separately from the device has been challenging since it deposits noncontinuously on glass substrates.[8,9]

Sb_2S_3 films were deposited on glass and on the HMTA film for 1 h by use of $SbCl_3$ and sodium thiosulfate precursors at 5 °C.[33] On glass, noncontinuous sparse nodules were obtained as expected (Figure 8a). On the HMTA seed layer, a 100 nm thick uniform Sb_2S_3 film was obtained (Figure 8b). The continuity of the film was confirmed with surface XPS analysis (Figure 8c). Sb_2S_3 on the seed layer has sharp Sb $3d_{5/2}$ and $3d_{3/2}$ peaks (at 528 and 534 eV, respectively) as well as S 2p peak (162 eV, not shown), but the Zn LMM (~500 eV) and Zn 3p peaks (88 eV) from the underlying seed layer are absent. The surface of Sb_2S_3 on glass shows the presence of Si 2p peak (103 eV) and is evidently noncontinuous. Use of the HMTA film as a nucleation layer opens up possibilities for versatile depositions of continuous and uniform sulfide films.

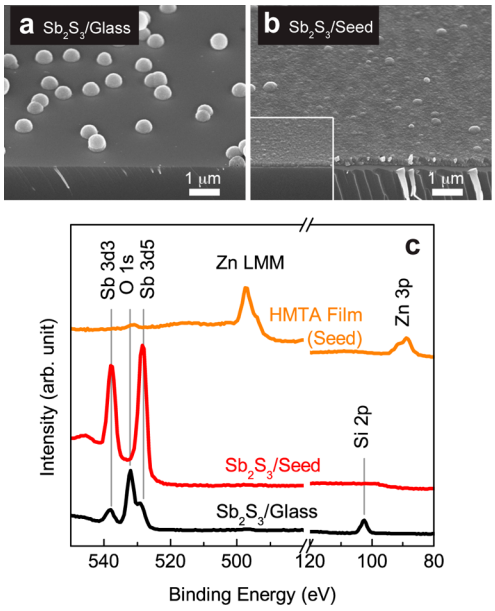

Figure 8. SEM 45° tilt views of Sb_2S_3 (a) on glass and (b) on HMTA film serving as a seed layer. (Inset) Seed layer without Sb_2S_3. Deposition on glass resulted in nodular morphology and non-continuous coverage, whereas a 100 nm thick continuous film was formed on top of the seed layer. The continuousness of the Sb_2S_3 film on the seed layer is evident by the absence of Zn LMM (500 eV) and Zn 3p (88 eV) peaks from (c) the surface XPS spectrum. The noncontinuousness of the Sb_2S_3/glass sample is confirmed by the presence of the Si 2p peak (103 eV).

Role of Hexamethylenetetramine. In this work, we have shown that addition of HMTA to the bath led to faster nucleation and growth of Zn(S,O,OH) film. To demonstrate whether pH difference is the sole cause for higher deposition rate, the standard bath was titrated with an external hydroxide source to mimic the pH profile of the HMTA bath, as adapted from the method of McPeak et al.[19] for ZnO deposition. The buffer 2-(*N*-morpholino)ethanesulfonic acid (MES) was used and the bath was continuously stirred to prevent sudden pH changes and inhomogeneity. The initial bath pH was adjusted to 5.2 at 90 °C, and the bath was titrated over time with 1.0 M KOH to match the pH profile of the HMTA bath. The changes in bath volume and ionic strength are minimal and are not expected to significantly affect the chemistries.[12,34] More details are provided in Supporting Information.

The titration bath yielded no films on a glass substrate as observed by SEM. As mentioned, without heterogeneous nucleation or attachment of nuclei, no films can be deposited. To put aside nucleation limitations, Zn(S,O,OH) film from the HMTA bath was used as a nucleation layer. If the growth rate of the HMTA bath were fully mimicked, ~90 nm of film would be added. However, only 32 ± 4 nm of additional film was deposited (see Figure S4 in Supporting Information), and dried precipitate mass was also less than that of the HMTA bath. Since HMTA slowly decomposes to ammonia, titration with an external ammonia source in place of KOH was also performed, and similar results were obtained. The titration film thickness is still considerably higher than 12 nm deposited by the standard bath for the same time. Thus, pH plays an important role in film growth rate as we have stipulated, but the presence of HMTA accelerates growth beyond simply the pH effects.

Growth acceleration occurs when the kinetics of the rate-determining step have changed or other film formation pathways have been competitively promoted. Since HMTA does not bind with Zn^{2+} ion in the bath,[13] HMTA may be involved in the transition state of the Zn-TAA reaction or directly with the decomposition of TAA. A comprehensive study on the possible reaction pathways of TAA was discussed by Bayón et al.[35] for deposition of $In(OH)_xS_y$. Pathways for the analogous Zn(S,O,OH) system are shown in Scheme 1. The direct reaction governing the rate of the standard bath is represented in pathway A, where TAA or thioacetoimide tautomers react directly with free Zn^{2+} ions for solid formation. TAA can also decompose either directly to provide S^{2-} ion, as in pathway B, or to thioacetic acid (TAC) intermediate before further decomposing to provide S^{2-} ion, as in pathway C. It is worth noting that a mechanism entailing $Zn(OH)_2$ nucleation, as we have observed for the ammoniac deposition of Zn(S,O,OH),[11] appears unlikely. $Zn(OH)_2$ and ZnO phases are undersaturated, as determined by speciation modeling by use of PHREEQC[36] software and stability constants available from NIST[37] (more details are provided in Supporting Information). Hence no nucleation or growth by $Zn(OH)_2$ or ZnO phases is possible regardless of the presence of HMTA.

Since the HMTA bath yielded more film and precipitate than the titration bath, its bath TAA concentration is likely to decrease more rapidly with time. Figure 9 shows time-resolved ATR-FTIR spectra of the HMTA bath and the titration bath. The range 950−1050 cm^{-1} is ideal for monitoring HMTA and

DOI: 10.1021/acsami.5b02482
ACS Appl. Mater. Interfaces 2015, 7, 11516−11525

Scheme 1. Pathways for Reaction of Thioacetamide in Acidic and Near-Neutral Media[a]

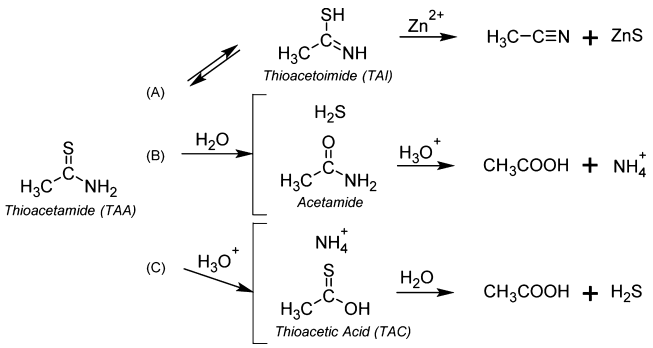

[a](A) TAA tautomerizes to thioacetoimide, and both can react with Zn^{2+} directly to form ZnS. (B) TAA hydrolyzes to acetamide and sulfide ion and then further decomposes to acetic acid and ammonia. (C) TAA hydrolyzes to thioacetic acid (TAC) and then further decomposes to acetic acid and sulfide ion. Adapted from ref 35.

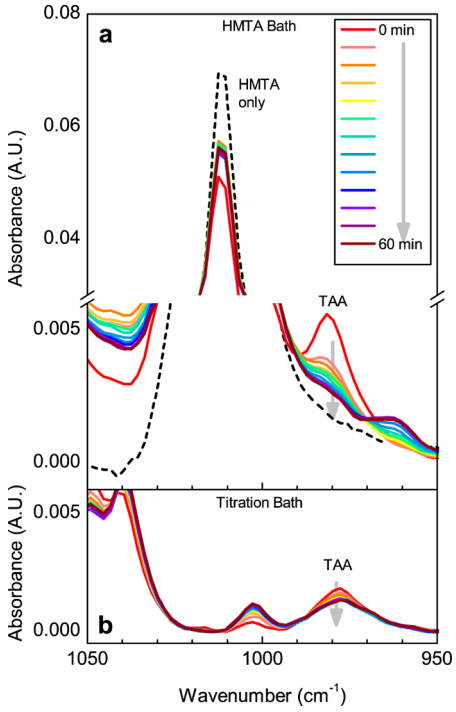

Figure 9. FTIR spectra of (a) HMTA bath and (b) titration bath. TAA peak decays more rapidly in the HMTA bath than in the titration bath. Dashed line shows the spectrum of 0.30 M HMTA solution.

TAA concentrations, as the signal-to-noise ratio is excellent and the water baseline varies slowly and is thus easy to subtract. The peak at ~1010 cm^{-1} is due to N−C stretching of HMTA,[38] whereas the peak centered ~980 cm^{-1} is due to CH_3 rocking of TAA.[39,40] The aliquot at time zero might have been sampled before mixing is fully homogeneous, as denoted by the unusually high TAA peak and the unusually low HMTA peak. Nevertheless, the rate of decay of the TAA peak from 5 min onward is more rapid for the HMTA bath than the titration bath. Overall, ~60% of the TAA decayed in the HMTA bath as compared to ~19% in the titration bath, ~3× faster over 1 h reaction time.

The fast disappearance of TAA in the HMTA bath confirms the accelerated reaction but is insufficient for concluding the specific role of HMTA. Variation in other parameters could further elucidate the role. If HMTA accelerates the direct Zn-TAA reaction (pathway A), reaction rate should be a function of TAA, HMTA, and Zn^{2+} concentrations, and a reduction in initial Zn^{2+} concentration should result in a slower TAA disappearance rate. Similar FTIR analysis was done on an HMTA bath with 10× less $ZnSO_4$ (and NTA). Its pH profile and TAA disappearance rate are similar to the regular HMTA bath and are independent of Zn^{2+} concentration, which indicates not only that HMTA dominantly controls pH but also that HMTA does not accelerate the direct reaction in pathway A (see Figure S5 in Supporting Information).

The fast consumption of TAA in the HMTA bath can lead to solids formation through accelerated hydrolysis of TAA, releasing more S^{2-}, which leads to larger degree of supersaturation of ZnS by pathways B or C. Total sulfide ion concentration in the HMTA bath and titration bath were recorded following the method reported in Opasanont et al.,[11] using a sulfide ion-selective electrode. For each bath, the sulfide concentration is 6×10^{-5} M initially. This value is used to calculate the supersaturation index (SI) of the ZnS phase with the free Zn^{2+} ion concentration determined from the PHREEQC speciation software according to

$$\mathrm{SI(ZnS)} = \log_{10}\left(\frac{[\text{free } Zn^{2+}][S^{2-}]}{K_{sp,ZnS}}\right)$$

where K_{sp} is the solubility product, corrected to the bath temperature by use of the van't Hoff equation. Since the pH and concentrations of total Zn^{2+} ion and NTA are identical between the two baths, the free Zn^{2+} ion concentration is similar, and the SI(ZnS) are equal at 6.3. The ion condensation pathway has the same impact on the film nucleation in the two baths, no matter how small. Its impact on film growth acceleration, or lack thereof, is more apparent with its time dependency. Figure 10 shows that the total sulfide concentration decreased with time for the HMTA bath but increased for the titration bath. The HMTA bath also has less total Zn^{2+} ion in the bath at any one time than the titration bath since more solids were formed. Thus, SI(ZnS) for the HMTA bath is always lower than for the titration bath. This inversion of SI compared to their relative growth rates is strong evidence that pathway B is not significantly accelerated by the presence of HMTA and that another pathway was competitively consuming TAA.

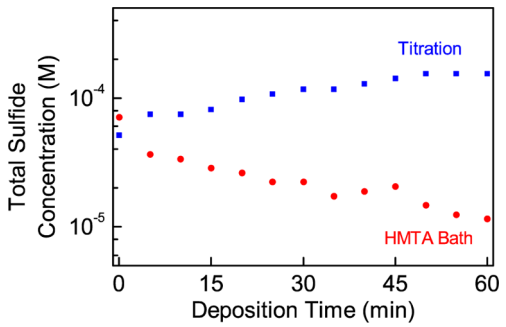

Figure 10. Total sulfide concentration in HMTA and titration baths as measured by a sulfide ion-selective electrode.

Given that TAA disappears faster in the presence of HMTA (Figure 9) but does not react faster directly with Zn^{2+} or lead to

DOI: 10.1021/acsami.5b02482
ACS Appl. Mater. Interfaces 2015, 7, 11516−11525

accumulation of S^{2-} ions (Figure 10), the likely promoted pathway is C, involving an intermediate. In this case, the decomposition of TAA to TAC (or other intermediates) is accelerated by HMTA, followed by fast reaction of the intermediate(s) with Zn^{2+} ions to form ZnS solids. Quantification of TAC in the bath by FTIR was not reliable, as the TAC peaks in aqueous solution are relatively weak and are situated on the shoulder of the HMTA peak. It is plausible that the intermediate(s) contain C and N (such as thiocyanate), as detected in the film composition analysis by XPS (Figure 3).

SUMMARY AND CONCLUSIONS

Chemical bath deposition in the near-neutral pH regime allows Zn(S,O,OH) thin films with low oxygen content to be deposited. However, the deposition rate is low due to consumption of hydroxide by the thioacetamide (TAA) sulfur source, leading to reduced pH and reaction rate. Hexamethylenetetramine (HMTA) was added to maintain high pH for faster reaction kinetics. Thin films deposited with HMTA additives were continuous, uniform, and well-adherent to glass, FTO, and $Cu_2(Zn,Sn)Se_4$ substrates. HMTA is believed to catalyze the decomposition of TAA to reactive S-containing intermediate(s) in addition to maintaining high pH. Regardless of specific reaction mechanism, we have demonstrated a novel chemistry for deposition of Zn(S,O,OH) thin films with higher growth rates, transparency, resistivity, and adhesion to serve as a nucleation layer or an extremely thin continuous coating for thin film applications. Strategic use of HMTA may also lead to improved solution processing and film properties for other metal chalcogenides and oxides.

ASSOCIATED CONTENT

Supporting Information

Additional text, five figures, and three tables showing XPS spectra of HMTA film on CZTSe, supporting grazing-incidence XRD data, titration experiment details, FTIR spectra of HMTA bath with less Zn^{2+} concentration, bath sulfide concentration measurement, and chemical bath speciation modeling. The Supporting Information is available free of charge on the ACS Publications website at DOI: 10.1021/acsami.5b02482.

AUTHOR INFORMATION

Corresponding Author

*E-mail jbaxter@drexel.edu.

Notes

The authors declare no competing financial interest.

ACKNOWLEDGMENTS

J.B.B. acknowledges support from the National Science Foundation (NSF) through Award CMMI-1000111. We are grateful to Dr. Kevin T. Turner at the University of Pennsylvania for advice on adhesion testing, to Melissa C. Santos and Dr. Yossef A. Elabd for assistance with ATR-FTIR measurements, to Andrew Dillon and Dr. Aaron T. Fafarman for assistance with resistivity measurements, to Nutte Teraphongphom and Dr. Margaret A. Wheatley for assistance with UV−vis measurements, and to Drexel University Core Facilities for their instrumentation support, especially to Dr. Edward Basgall for assistance with thermal evaporation.

REFERENCES

(1) Hodes, G. *Chemical Solution Deposition of Semiconductor Films*; CRC Press: Boca Raton, FL, 2003.
(2) Witte, W.; Abou-Ras, D.; Hariskos, D. Chemical Bath Deposition of Zn(O,S) and CdS Buffers: Influence of Cu(In,Ga)Se_2 Grain Orientation. *Appl. Phys. Lett.* **2013**, *102*, 051607.
(3) Nielsen, A. E. *Kinetics of Precipitation*; Pergamon Press: New York, 1964.
(4) Smet, P. F.; Moreels, I.; Hens, Z.; Poelman, D. Luminescence in Sulfides: A Rich History and a Bright Future. *Materials* **2010**, *3*, 2834−2883.
(5) Bhattacharya, R. N.; Contreras, M. A.; Teeter, G. 18.5% Copper Indium Gallium Diselenide (CIGS) Device Using Single-Layer, Chemical-Bath-Deposited ZnS(O,OH). *Jpn. J. Appl. Phys.* **2004**, *43*, L1475−L1476.
(6) Ennaoui, A.; Bär, M.; Klaer, J.; Kropp, T.; Sáez-Araoz, R.; Lux-Steiner, M. C. Highly-Efficient Cd-Free $CuInS_2$ Thin-Film Solar Cells and Mini-Modules with Zn(S,O) Buffer Layers Prepared by an Alternative Chemical Bath Process. *Prog. Photovoltaics* **2006**, *14*, 499−511.
(7) Yamaguchi, K.; Yoshida, T.; Lincot, D.; Minoura, H. Mechanistic Study of Chemical Deposition of ZnS Thin Films from Aqueous Solutions Containing Zinc Acetate and Thioacetamide by Comparison with Homogeneous Precipitation. *J. Phys. Chem. B* **2003**, *107*, 387−397.
(8) Maghraoui-Meherzi, H.; Ben Nasr, T.; Kamoun, N.; Dachraoui, M. Structural, Morphology and Optical Properties of Chemically Deposited Sb_2S_3 Thin Films. *Phys. B (Amsterdam, Neth.)* **2010**, *405*, 3101−3105.
(9) Lokhande, C.; Sankapal, B.; Mane, R.; Pathan, H.; Muller, M.; Giersig, M.; Ganesan, V. XRD, SEM, AFM, HRTEM, EDAX and RBS Studies of Chemically Deposited Sb_2S_3 and Sb_2Se_3 Thin Films. *Appl. Surf. Sci.* **2002**, *193*, 1−10.
(10) Persson, C.; Platzer-Björkman, C.; Malmström, J.; Törndahl, T.; Edoff, M. Strong Valence-Band Offset Bowing of $ZnO_{1-x}S_x$ Enhances P-Type Nitrogen Doping of ZnO-like Alloys. *Phys. Rev. Lett.* **2006**, *97*, No. 146403.
(11) Opasanont, B.; Kuba, A. G.; Louderback, E. G.; Roy Choudhury, K.; Baxter, J. B. Relating Deposition Conditions to Zn(S,O,OH) Thin Film Properties for Photovoltaic Buffer Layers Using a Continuous Flow Microreactor. *Chem. Mater.* **2014**, *26*, 6674−6683.
(12) Bowersox, D. F.; Smith, D. M.; Swift, E. H. The Precipitation of Zinc Sulphide from Acid Solutions by Thioacetamide. *Talanta* **1960**, *3*, 282−295.
(13) McPeak, K. M.; Becker, M. A.; Britton, N. G.; Majidi, H.; Bunker, B. A.; Baxter, J. B. In Situ X-Ray Absorption Near-Edge Structure Spectroscopy of ZnO Nanowire Growth during Chemical Bath Deposition. *Chem. Mater.* **2010**, *22*, 6162−6170.
(14) Cao, Y.; Denny, M. S.; Caspar, J. V.; Farneth, W. E.; Guo, Q.; Ionkin, A. S.; Johnson, L. K.; Lu, M.; Malajovich, I.; Radu, D.; Rosenfeld, H. D.; Choudhury, K. R.; Wu, W. High-Efficiency Solution-Processed $Cu_2ZnSn(S,Se)_4$ Thin-Film Solar Cells Prepared from Binary and Ternary Nanoparticles. *J. Am. Chem. Soc.* **2012**, *134*, 15644−15647.
(15) Goudarzi, A.; Aval, G. M.; Sahraei, R.; Ahmadpoor, H. Ammonia-Free Chemical Bath Deposition of Nanocrystalline ZnS Thin Film Buffer Layer for Solar Cells. *Thin Solid Films* **2008**, *516*, 4953−4957.
(16) Shin, S. W.; Kang, S. R.; Gurav, K. V.; Yun, J. H.; Moon, J.-H.; Lee, J. Y.; Kim, J. H. A Study on the Improved Growth Rate and Morphology of Chemically Deposited ZnS Thin Film Buffer Layer for Thin Film Solar Cells in Acidic Medium. *Sol. Energy* **2011**, *85*, 2903−2911.
(17) McPeak, K. M.; Opasanont, B.; Shibata, T.; Ko, D.-K.; Becker, M. A.; Chattopadhyay, S.; Bui, H. P.; Beebe, T. P.; Bunker, B. A.; Murray, C. B.; Baxter, J. B. Microreactor Chemical Bath Deposition of Laterally Graded $Cd_{1-x}Zn_xS$ Thin Films: A Route to High-Throughput Optimization for Photovoltaic Buffer Layers. *Chem. Mater.* **2013**, *25*, 297−306.

DOI: 10.1021/acsami.5b02482
ACS Appl. Mater. Interfaces 2015, 7, 11516−11525

(18) López, G. P.; Castner, D. G.; Ratner, B. D. XPS O 1s Binding Energies for Polymers Containing Hydroxyl, Ether, Ketone and Ester Groups. *Surf. Interface Anal.* **1991**, *17*, 267−272.
(19) McPeak, K. M.; Le, T. P.; Britton, N. G.; Nickolov, Z. S.; Elabd, Y. A.; Baxter, J. B. Chemical Bath Deposition of ZnO Nanowires at Near-Neutral pH Conditions without Hexamethylenetetramine (HMTA): Understanding the Role of HMTA in ZnO Nanowire Growth. *Langmuir* **2011**, *27*, 3672−3677.
(20) Wei, S.; Zunger, A. Band Offsets and Optical Bowings of Chalcopyrites and Zn-based II-VI Alloys. *J. Appl. Phys.* **1995**, *78*, 3846−3856.
(21) Williamson, G. K.; Hall, W. H. X-Ray Line Broadening from Filed Aluminium and Wolfram. *Acta Metall.* **1953**, *1*, 22−31.
(22) Zhang, H.; Chen, B.; Gilbert, B.; Banfield, J. F. Kinetically Controlled Formation of a Novel Nanoparticulate ZnS with Mixed Cubic and Hexagonal Stacking. *J. Mater. Chem.* **2006**, *16*, 249−254.
(23) Dona, J. M.; Herrero, J. Process and Film Characterization of Chemical-Bath-Deposited ZnS Thin Films. *J. Electrochem. Soc.* **1994**, *141*, 205−210.
(24) Danaher, W. J.; Lyons, L. E.; Morris, G. C. Some Properties of Thin Films of Chemically Deposited Cadmium Sulphide. *Sol. Energy Mater.* **1985**, *12*, 137−148.
(25) Padam, G. K.; Malhotra, G. L.; Rao, S. U. M. Studies on Solution- grown Thin Films of $Zn_xCd_{1-x}S$. *J. Appl. Phys.* **1988**, *63*, 770−774.
(26) Turner, K. T.; Spearing, S. M. Accurate Characterization of Wafer Bond Toughness with the Double Cantilever Specimen. *J. Appl. Phys.* **2008**, *103*, 013514.
(27) Maszara, W. P.; Goetz, G.; Caviglia, A.; McKitterick, J. B. Bonding of Silicon Wafers for Silicon-on-insulator. *J. Appl. Phys.* **1988**, *64*, 4943−4950.
(28) Bradt, R. C.; Munz, D.; Sakai, M.; White, K. W. *Fracture Mechanics of Ceramics*; Springer: Boston, MA, 2005.
(29) Kinloch, A. J. *Adhesion and Adhesives: Science and Technology*, 1st ed.; Springer Science & Business Media: London, 1987.
(30) Yoon, T.; Shin, W. C.; Kim, T. Y.; Mun, J. H.; Kim, T.-S.; Cho, B. J. Direct Measurement of Adhesion Energy of Monolayer Graphene As-Grown on Copper and Its Application to Renewable Transfer Process. *Nano Lett.* **2012**, *12*, 1448−1452.
(31) Itzhaik, Y.; Niitsoo, O.; Page, M.; Hodes, G. Sb_2S_3-Sensitized Nanoporous TiO_2 Solar Cells. *J. Phys. Chem. C* **2009**, *113*, 4254−4256.
(32) Messina, S.; Nair, M. T. S.; Nair, P. K. Solar Cells with Sb_2S_3 Absorber Films. *Thin Solid Films* **2009**, *517*, 2503−2507.
(33) Messina, S.; Nair, M.; Nair, P. Antimony Sulfide Thin Films in Chemically Deposited Thin Film Photovoltaic Cells. *Thin Solid Films* **2007**, *515*, 5777−5782.
(34) Peeters, O. M.; de Ranter, C. J. Pathways in Thioacetamide Hydrolysis in Aqueous Acid: Detection by Kinetic Analysis. *J. Chem. Soc., Perkin Trans. 2* **1974**, 1832−1835.
(35) Bayón, R.; Herrero, J. Solution Chemistry and Reaction Mechanism Taking Place during the Chemical Bath Deposition of $In(OH)_xS_y$. In *Chemical Solution Deposition of Semiconducting and Non-metallic Films*; The Electrochemical Society, Inc: Paris, 2003; Vol. *32*, pp 73−81.
(36) Parkhurst, D. L.; Appelo, C. A. J. *User's Guide to PHREEQC (version 2)--A Computer Program for Speciation, Batch-Reaction, One-Dimensional Transport, and Inverse Geochemical Calculations*; U.S. Geological Survey Water-Resources Investigations Report 99-4259; 1999.
(37) Smith, R. M.; Martell, A. E. *NIST Critically Selected Stability Constants of Metal Complexes*; NIST Standard Reference Database 46; National Institute of Standards and Technology: Gaithersburg, MD, 2004.
(38) Jensen, J. O. Vibrational Frequencies and Structural Determinations of Hexamethylenetetraamine. *Spectrochim. Acta, Part A* **2002**, *58*, 1347−1364.
(39) Suzuki, I. Infrared Spectra and Normal Vibrations of Thioamides. II. Thioacetamide. *Bull. Chem. Soc. Jpn.* **1962**, *35*, 1449−1456.
(40) Kutzelnigg, W.; Mecke, R. Spektroskopische Untersuchungen an Organischen ionen—III: Das Infrarot-Spektrum Und Die Struktur Des Thiohamstoff-Kations (thiouromum-Ions), Des S-methyIthiouromum-Ions, Des Thioacetamid-Kations Und Des Thioacetamid-kupfer(I)-chlorid-Komplexes. *Spectrochim. Acta* **1961**, *17*, 530−544.

DOI: 10.1021/acsami.5b02482
ACS Appl. Mater. Interfaces 2015, 7, 11516−11525